K^0_S and Λ production from proton-proton collisions at the LHC with ALICE

Barnaby Howells
Student No: 2130309
Project Partner: Thomas Ferguson
Supervisors: Prof. D. Evans and Dr R. Lietava

Y4 Project Final Report
March 2024

Abstract

This report presents analysis of the singly strange K^0_S meson and Λ baryon, produced during proton-proton collisions from the ALICE experiment at the LHC. It serves as a preliminary check on new data collected during ALICE Run 3, which began in 2022. Selection cuts were applied to improve the purity of the data sample, and reconstruction efficiencies for both particles were calculated using Monte Carlo simulations. These are used to correct their transverse momentum spectra, allowing for the baryon to meson (Λ/K^0_S) ratio to be calculated. The efficiencies peaked at 0.08 and 0.09 for the K^0_S and Λ respectively, a factor of three lower than expected from previous results. The Λ/K^0_S ratio settled at 0.3 in the mid transverse momentum range and increased dramatically at low transverse momentum, compared with a peak of 0.6 obtained from Run 2 analysis. Systematic errors relating to cut selection are discussed, along with other potential sources of these discrepancies.

Contents

1 Introduction

The ALICE (A Large Ion Collider Experiment) collaboration at the Large Hadron Collider (LHC) was proposed in 1993 as a means to study the physics of a strongly interacting phase of matter called Quark Gluon Plasma (QGP), by colliding combinations of protons (p) and lead (Pb) nuclei together at relativistic speeds [1]. In doing so, ALICE recreates the conditions believed to be present shortly after the big bang, where quarks and gluons, the fundamental building blocks of hadrons such as protons and neutrons, are no longer confined within particles. Instead, they move freely, resembling a hot and dense soup of particles. Due to its short lifetime, QGP is not observable directly, and therefore several signatures are used to infer its properties. One such signature involves analysing the production of strange hadrons, composite particles containing at least one strange quark or anti-quark, across different types of collisions. Strange hadrons are particularly sensitive to the conditions of the QGP medium and exhibit patterns in their production rates which provide valuable insights into its nature.

This project will focus on the production of two strange particles from proton-proton (pp) collisions: the K-zero-short (K^0_S) meson and the Lambda (Λ) baryon. Both particles are neutral and contain a single strange quark. The K^0_S is comprised of a down quark and a strange anti-quark ($d\bar{s}$), while the Λ contains a strange quark and a single up and down quark (uds). Both particles weakly decay into a positively and negatively charged particle, which creates distinctive 'V' shape tracks in the detector, hence they are collectively referred to as V^0s. These particles play a crucial role in the ALICE experiment, as they serve as probes for the properties of the QGP produced in heavy ion collisions. However, QGP is not expected to form during the pp collisions analysed during this project, as the collision is too short-lived for the phase transition to QGP to occur. This means that the interactions resulting from pp collisions are purely hadronic and are typically used as QGP-absent baselines to compare to heavy ion collision data [2], hence this project does not aim to study the effects of QGP directly.

Since V^0s are neutral, they escape direct detection, and therefore must be reconstructed from their decay products, also known as their daughters. For K^0_S, the most common decay products are two charged pions (π^+ and π^-), while Λ typically decays into a proton and pion (p and π^-). Since pions, composed of combinations of up and down (anti-)quark pairs, are the lightest mesons, they are produced abundantly during collisions, and must be analysed to determine whether they originated from a V^0 decay. Throughout this report, the word 'candidates' will be used to refer to reconstructed particle tracks identified as potential instances of a V^0 particle. The total number of particles produced in a collision event is known as multiplicity, and is often used in particle physics as it provides information about the complexity of the collision. However, multiplicity data was unavailable for the duration of the project.

This project uses data collected during the most recent period of data collection at ALICE, which began in July 2022, known as Run 3. This run follows a shutdown period during which a number of key upgrades to ALICE components were made, allowing Pb-Pb collisions to be recorded at up to 50 times the rate compared to Run 2 [3]. The data collected during this run is still being assessed and is subject to further calibration. This project serves as a preliminary investigation of this new data, and comparisons to previous results will be made throughout. This report will introduce the relevant background theory, before detailing the methods used to carry out the project, and presenting and discussing the key results.

2 Background Theory

2.1 The Standard Model

The Standard Model is a comprehensive theoretical framework that unifies our understanding of three of the four fundamental forces of nature: the strong, weak, and electromagnetic forces [4]. It describes the interactions of different classes of particles, including quarks, which are the elementary constituents of protons and neutrons. Quarks come in six distinct 'flavours' of unique mass and charge: up, down, top, bottom, charm, and strange, with protons being comprised of two up and one down quark. Additionally, the Standard Model includes force-carrying particles such as photons and gluons, which mediate the fundamental forces. Hadrons, composite particles made up of quarks and gluons, are bound together by the strong force. There are two main types of hadrons: baryons, consisting of three quarks, and mesons, composed of a pair of quarks and anti-quarks, their anti-matter counterparts. Together, these particles and interactions form the foundation of our understanding of particle physics.

2.2 Quantum Chromodynamics

Quantum Chromodynamics (QCD) is a theory within the Standard Model that governs the action of the strong nuclear force [5]. In QCD, quarks are assigned a property called colour charge, which comes in three types: red, green, and blue, analogous to electrical charge in electromagnetism. Similarly, anti-quarks carry anti-colour charges. Hadrons are colour neutral, as each of a baryon's three quarks are of a different colour, and the anti-quarks effectively neutralise the colour charge of the quarks within mesons.

Similar to photons in electromagnetism, the strong force is mediated by the exchange of gluons, i.e. they act as the "glue" holding the quarks together. Crucially however, gluons also carry combinations of colour and anti-colour themselves. This enables them to self-interact and imposes restrictions on the existence of quarks and gluons in nature. In contrast to electromagnetism, as quarks separate, the strong force between them increases, leading to a rise in the potential energy of the system. As the distance increases, eventually it becomes energetically favourable for new quark-antiquark pairs to form spontaneously from the vacuum between them. This prevents individual colour-charged particles from existing in isolation and is known as confinement.

However, the strong force between quarks becomes weaker at shorter distances, or equivalently, higher energies. This phenomenon is known as asymptotic freedom and allows quarks and gluons to act almost as free particles at extreme energy densities, such as those created during collisions with ALICE. This leads to a phase transition to a QGP state, where interactions between quarks and gluons become weak enough for them to be liberated from their bound states within hadrons. It is believed that between 10^{-12} and 10^{-5} seconds after the big bang, the universe was in a QGP state [6]. Hence, by investigating QGP, ALICE may provide valuable insights into the limits of QCD and the evolution of the early universe.

3 ALICE

The following section describes details of the Large Hadron Collider (LHC) and the ALICE experimental setup, which enable the production and analysis of collision events. Particular attention will be given to the components of the ALICE detector used to identify the Λ and K^0_S particles.

3.1 The Large Hadron Collider

ALICE is located at the LHC particle accelerator at CERN in Switzerland [7]. Measuring 27 kilometres in circumference, the LHC is the world's largest and highest-energy particle accelerator. Particles are guided using magnetic fields maintained by a ring of superconducting electromagnets. At full speed, protons move at just 3.1 m/s slower than the speed of light, and complete 11,245 revolutions of the ring per second [8]. The LHC contains two adjacent beam pipes and collides them at four crossing points, surrounded by nine detectors each optimised to study different phenomena. Before describing the ALICE detector itself, it is convenient to define the coordinate system used to describe the motion and interaction of particles.

3.2 ALICE Coordinate System

ALICE studies the collision between two ultra-relativistic beams travelling in opposite directions, with the collision taking place at the centre of the ALICE detector. The point of collision is chosen as the reference point for defining the coordinate system and is known as the primary vertex. Any subsequent decays of particles produced during the collision may be referred to as secondary vertices. As shown in figure 1, the z-direction is defined to be parallel to the beam, with the x-y plane extending radially outwards from the primary vertex. Motion that occurs along the beam axis is said to be longitudinal, while perpendicular motion is described as transverse. It is useful to note a particle's transverse momentum, $p_T = \sqrt{p_x^2 + p_y^2}$, defined as the components of its momentum perpendicular to the beam. This report will ultimately present plots as functions of p_T, to evaluate detector performance and probe the behaviour of particles across momentum ranges.

Another key property of particles produced during collisions is the angle of their trajectory relative to the positive z-axis, θ. Instead of θ, it is preferred in particle physics to use the concept of pseudo-rapidity, η, defined as

$$\eta = -\ln\left[\tan\left(\frac{\theta}{2}\right)\right], \tag{1}$$

since differences in pseudo-rapidity are Lorentz invariant under boosts along the z-axis [9]. The detector is centred around $\eta = 0$ for particles travelling perpendicular to the beam, and approaches infinity as θ tends towards zero. This property makes pseudo-rapidity a convenient parameter to refer to when introducing the various components of the detector.

3.3 ALICE Detector

The ALICE detector [10], shown in figure 1, is optimised to measure heavy-ion collisions and study QGP. Located 56m below the ground, it extends 26m in length and 16m in height and width. It

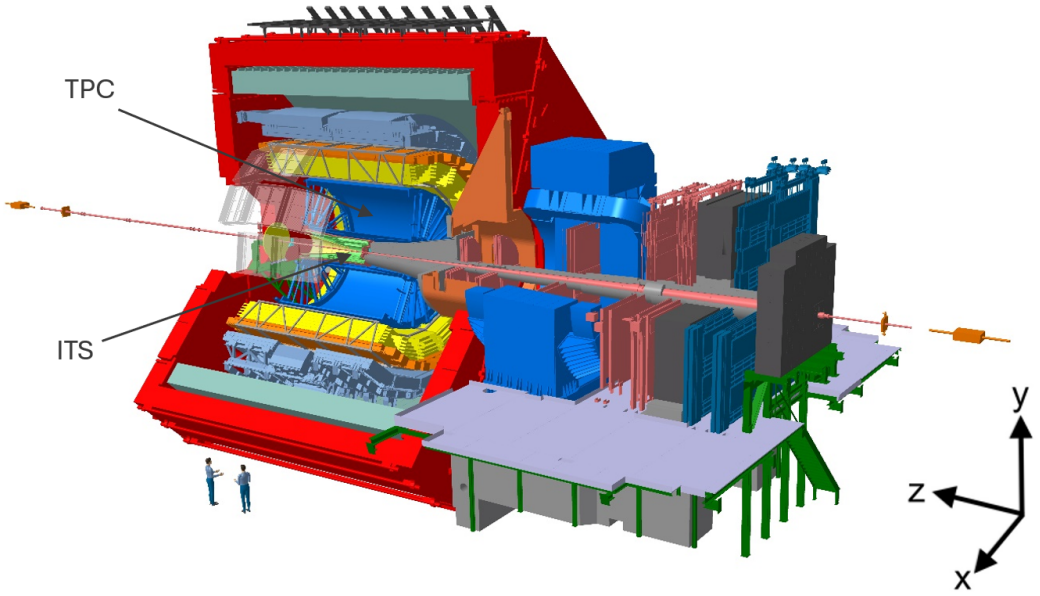

Figure 1: ALICE detector as in RUN3 [11].

features an array of sub-detectors, broadly separated into three categories: the central barrel, forward detectors and muon arm. Of these sub-detectors, only the Inner Tracking System (ITS) and Time Projection Chamber (TPC) will be discussed in detail, as they are the key components used to track and identify V^0 candidates. Both components are located in the central barrel, which extends outwards from the collision point. They are placed within an external magnetic field, which exerts a force on charged particles and allows for their momentum to be calculated from the radius of curvature of their tracks.

3.3.1 Inner Tracking System

The ITS serves as the initial detector encountered by mid-rapidity particles generated during collisions [12], with its innermost detection layer positioned 22.4mm away from the interaction point. It covers the region $|\eta| < 1.22$ (corresponding to $33° < \theta < 147°$) and extends approximately 0.4m away from the beam pipe. The primary role of the ITS is to determine the primary and secondary decay vertices to a high degree of precision. In addition, the ITS improves the resolution of low p_T particles and aids the momentum measurements made by the TPC. The ITS consists of seven layers of silicon pixels arranged cylindrically around the beam pipe, and can be further categorised into two sections. The first three layers form the inner barrel (IB), optimised to capture particles emerging directly from the collision point and facilitate precise vertexing. The remaining four layers constitute the outer barrel (OB), enhancing the tracking efficiency for particles with larger trajectories.

The ITS utilises Monolithic Active Pixel Sensor (MAPS) technology, which integrates both sensor and readout electronics on a single silicon substrate [13]. The silicon sensor layer interacts with charged particles passing through it, and is then segmented into an array of pixels, each one able to register the charge generated by ionising particles. This design results in a compact and highly efficient tracking device. Overall, the ITS is capable of reconstructing the primary vertex with

a precision as low as 2–3 µm for high multiplicity Pb-Pb collisions [14]. However, in the case of pp collisions, the resolution can drop off rapidly due to the lower multiplicity, since fewer particle tracks provide the ITS with less information and increase statistical uncertainty.

3.3.2 Time Projection Chamber

The TPC is a $90m^3$ cylinder filled with gas, which provides accurate Particle IDentification (PID), as well as complete tracking for particles over a wide range of momenta [15]. Charged particles that traverse the TPC ionise gas molecules along their path, freeing electrons in the process. An electrode at the centre of the chamber separates the cylinder into two regions, such that each electron drift towards the corresponding end plate. This signal is then amplified by Gas Electron Multipliers (GEM), which increase the number of electrons detected by creating a series of electron avalanches through perforated foil layers. The gas is comprised of a precise composition of neon, carbon dioxide and nitrogen, that must be optimised based on factors such as ion drift speed, material budget, and operational stability [16].

By measuring the specific ionisation energy loss (dE/dx) of particles as they traverse the TPC, it is possible to distinguish between different particle species. This is because particles with different masses and energies lose energy at different rates in the gas, leading to distinct dE/dx signatures [17]. By combining this information with the tracking information from the ITS, ALICE can perform PID over a wide range of momenta and particle types.

4 Data Analysis

The data analysis employed in this report follows established methodologies from previous runs. Initial steps involve applying a series of selection cuts to enhance the purity of the data by reducing background noise. The physical justifications for these cuts are discussed in detail, as well as their effectiveness at improving the quality of the overall data sample. Next, the reconstruction efficiencies of the detector are calculated using computer-generated (Monte Carlo) simulations. These efficiencies quantify the detector's ability to accurately reconstruct particle tracks, and allow the raw p_T spectra of each particle to be corrected for further analysis.

4.1 Event Selection

Since the Λ and K^0_S particle are both neutrally charged, they are not detected directly. Instead, they must be reconstructed from their weak decay products. As previously stated, the most common decay mode for each particle is $K^0_S \to \pi^+\pi^-$ and $\Lambda \to p\pi^-$, with branching ratios of 69% and 64% respectively. A series of informed selection cuts based on the decay topologies of both particles may be implemented, to increase the probability that any individual candidate originated from the decay of a V^0, and therefore reduce unwanted background. A diagram of a K^0_S decay with the possible cuts is shown in figure 2. For each candidate, five selection cuts are available, as listed below:

- **DCA between daughter tracks and primary vertex** - The Distance of Closest Approach (DCA) calculated between both the positive and negative daughter track and the primary vertex (PV), resulting in two individual cut selections. A candidate was excluded if it came

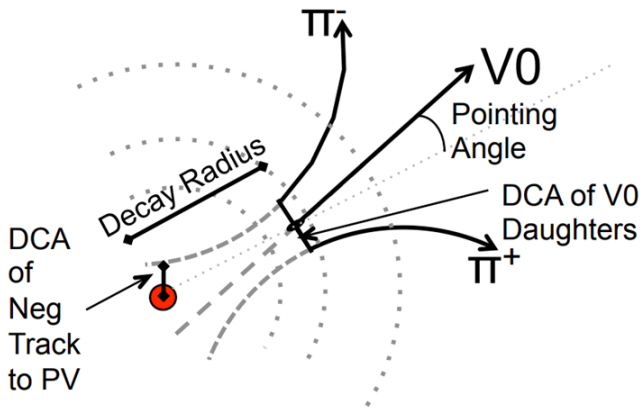

Figure 2: $K^0_S \to \pi^+\pi^-$ decay topology with available cuts [18].

too close to the primary vertex when reconstructed, to ensure the remaining particles were unlikely to have originated from the initial collision.

- **DCA between V^0 daughters** - The DCA between the positive and negative daughter tracks. To be consistent with a V^0 decay, both daughter tracks must have originated from the same vertex, within the resolution of the detector. Therefore, a maximum cut was implemented, excluding candidates whose daughters were unlikely to have originated from the same point.

- V^0 **Decay Radius** - Defined as the distance between the primary vertex and the decay vertex assigned to each of the V^0 candidates. The latter was defined as a point on the line connecting the V^0 daughters at their points of closest approach. A minimum cut was placed on this distance to ensure it was consistent with lifetimes of the V^0s.

- **Cosine of pointing angle** - The pointing angle refers to the angle between the momentum vector of the daughter tracks and the vector connecting the primary and V^0 decay vertices. A small pointing angle indicates good agreement between the reconstructed trajectory of the V^0 particle and the expected trajectory based on its decay vertex. A cut was placed on the cosine of this angle, removing candidates whose pointing angles were too large.

By default, these selection cuts were set to loose values. Each cut was then systematically tightened, while keeping the others constant. It was then returned to its default value before adjusting the next cut. After each cut was implemented, the significance of the resulting invariant mass plot for each particle was calculated. The significance, defined as

$$Significance = \frac{S}{\sqrt{S+B}}, \tag{2}$$

where S and B are signal and background respectively, serves as a quantitative measure of the effectiveness of each cut in enhancing the signal to background ratio. To obtain the signal and background levels, a fitting function was used on each mass plot. Specifically, a Gaussian function was used to fit the peak, and a 2^{nd} order polynomial was used to fit the background signal. The fit was then integrated over a 5σ region around the peak, using the value of σ returned by the Gaussian fit. An example of a fitted mass plot for both particles is shown in figure 3, along with

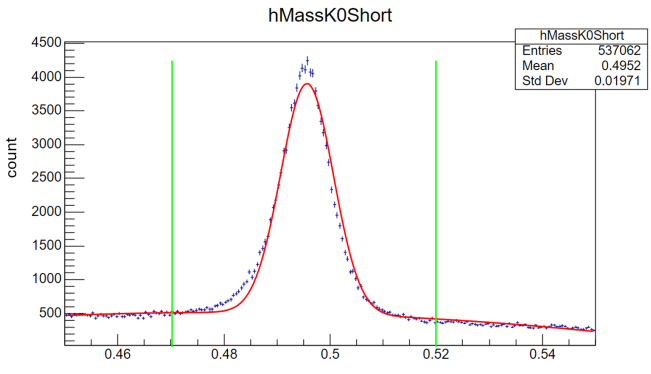

(a) K^0_S ($\pi^+\pi^-$) Invariant Mass Plot [GeV/c^2].

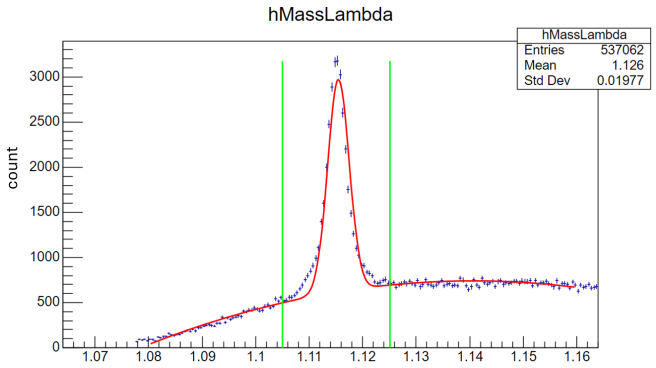

(b) Λ ($p\pi^-$) Invariant Mass Plot [GeV/c^2].

Figure 3: V^0 mass plots with fit. The 5σ range used for signal extraction is shown in green.

the range used for signal extraction.

Finally, the significance was plotted against cut value, with the optimal cut location assumed to correspond to the point of maximum significance. However, in addition to maximising significance, two additional factors were considered: the amount of signal retained by each cut, and the consistency between the real data and Monte Carlo (MC) simulations, to ensure the simulations correctly replicated the effects of the cuts on the V^0 yields. To achieve this, the fraction of signal retained by each cut was plotted below, on the same axis. Additionally, the same selection cuts were applied to the MC data, and the resulting signal retention was also plotted alongside the real data, allowing for direct comparisons between their behaviours. A cut was deemed acceptable if it retained at least 90% of the signal, whilst showing a discrepancy of no more than 2% between the real and MC data. An example of a significance plot for the K^0_S particle and the DCA between the positive particle and the primary vertex is shown in figure 4.

As seen in the figure, at the point where significance is maximised, approximately 98% of the initial signal is retained and the behaviour of the data is well described by the MC simulations, therefore the cut was accepted. By repeating this analysis for all five cuts and both particles, the final cut values, shown in table 1, were chosen.

Cut Values	K^0_S	Λ
DCA neg to PV [cm]	>0.101	>0.181
DCA pos to PV [cm]	>0.106	>0.050
DCA V^0 daughters [cm]	<0.205	<0.250
Cosine of pointing angle	>0.993	>0.990
V^0 radius [cm]	>0.9	>1.4

Table 1: Final cut values chosen.

To assess the impact of these selection criteria on the dataset, the invariant mass plots before and after implementing the cuts are compared in figure 5, for both particles. The plots depict the impact of the loose (blue) versus final (red) cuts. This visualisation reveals a clear reduction in background noise for both particles, while retaining the signal peak. Signal extraction from the refined mass plots indicate that each set of cuts retained 89% and 86% of the initial signal, for K^0_S

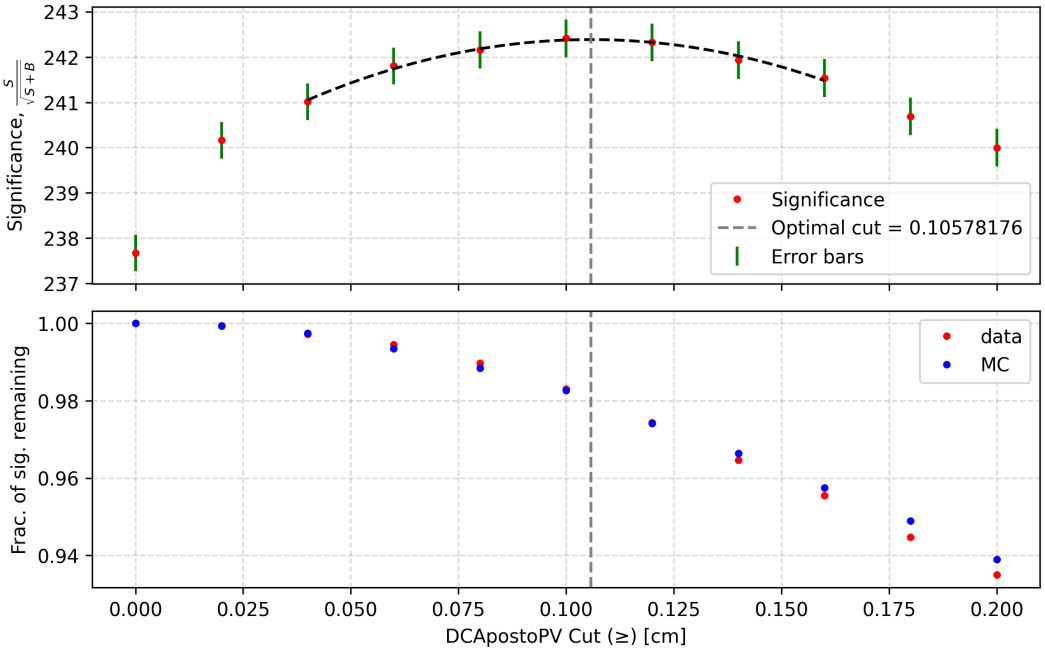

Figure 4: Significance of K^0_S mass plot and signal fraction remaining against DCA positive to PV cut. The grey dotted line indicates the point at which significance was maximised.

and Λ respectively, compared to 35% and 28% of the background. This is strong evidence that these cuts have worked as intended, enhancing the purity of the dataset and thereby improving the accuracy of subsequent analyses.

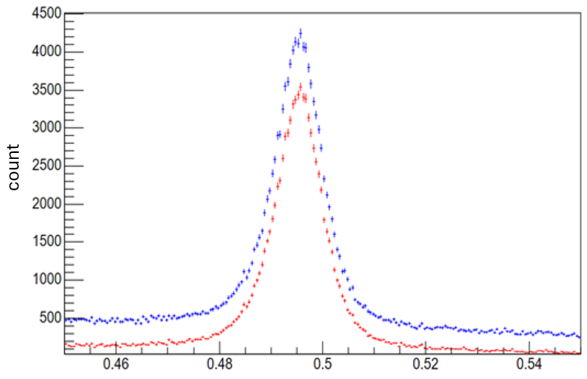

(a) K^0_S ($\pi^+\pi^-$) Invariant Mass Plot [GeV/c^2].

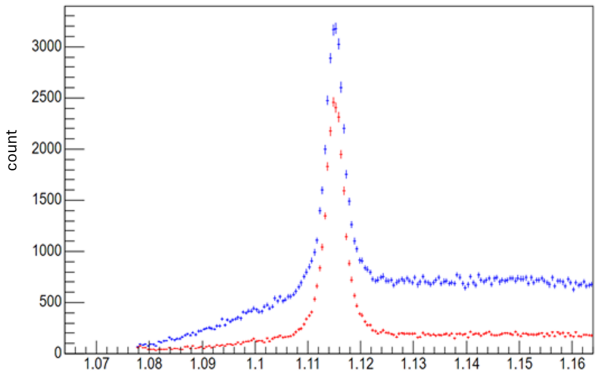

(b) Λ ($p\pi^-$) Invariant Mass Plot [GeV/c^2].

Figure 5: V^0 mass plots resulting from loose cuts (blue) and finalised cuts (red).

4.2 V^0 Reconstruction Efficiencies

In collision event analysis, the reconstruction efficiency refers to the proportion of produced particles that are successfully identified by the detector system. It provides a quantitative measure of detector performance and enables the raw momentum spectra of each particle to be corrected. Calculating these efficiencies involves simulating the entire experimental setup and particle interactions using computer-generated events.

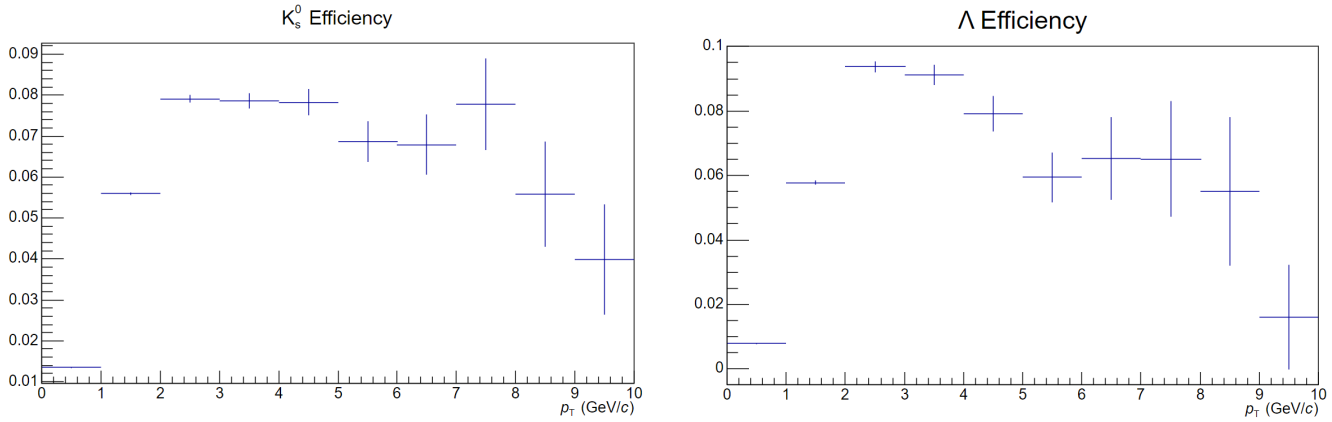

(a) K^0_S efficiency data.

(b) Λ efficiency data.

Figure 6: V^0 efficiency against p_T. Bin size has been increased for clarity.

Monte Carlo simulations begin by generating a large number of simulated collision events based on theoretical models or known physical processes. The particles produced from these events and their subsequent interactions are then processed through a detailed simulation of the detector geometry, accounting for factors such as the thickness and material composition of the detector components. The particle trajectories and the response of tracking detectors are then replicated, to obtain the simulated data, which is processed using the same reconstruction algorithms employed in the actual experimental data analysis.

Once this process is complete, the simulated events are analysed to determine how many of the generated particles are successfully identified by the reconstruction algorithms. The advantage of using MC simulations, is that the number of particles initially produced is known. This allows the ratio of successfully reconstructed particles to the total number of generated particles in each transverse momentum range to be calculated, providing the efficiency as a function of p_T for each particle of interest. The calculated efficiencies for the K^0_S and Λ particles are shown in figure 6.

The efficiency distributions for both particles follow a similar shape, with the detector performing poorly at low p_T. This is attributed partly to kinematic limitations, since low p_T particles may not reach the outer detectors effectively. The efficiencies then increase to a peak of around 0.08 for K^0_S and 0.09 for Λ, in the mid p_T range, meaning that just under 10% of the particles produced in this range are reconstructed correctly. Further discussion of these efficiencies, including comparisons to efficiencies obtained from previous runs, will be made later. Assuming the real data is well described by the MC, the raw momentum spectra for each particle may be divided by their respective efficiencies, to obtain the corrected spectra of particles produced in the collision, presented as part of the results.

5 Results

In this section, the corrected spectra of K^0_S and Λ obtained during this analysis will be presented and discussed in the context of the results obtained from previous runs. Using these corrected spectra, the baryon to meson ratio is calculated by dividing the Λ spectra by the K^0_S spectra. This

can provide a useful insight into physical phenomena when compared between different collision types. For this project, it serves as a means to cross-check the results with previous pp collision data, thereby assessing the accuracy of the findings.

5.1 Corrected Spectra

The corrected spectra for K^0_S and Λ are shown in figure 7, using both linear and a logarithmic scales. Clearly, the majority of the particles are produced at low p_T, with both distributions falling exponentially at high p_T.

The K^0_S yield is seen to increase to a maximum around 0.5 GeV/c, which is consistent with what is expected from previous results [18]. The point of inflection for the K^0_S curve occurs at just under 1 GeV/c. Conversely, the Λ yield exhibits continuous growth at lower p_T, without any discernible turning point. The logarithmic plot in figure 7d more clearly shows the Λ spectra at low p_T, which is observed to increase by several orders of magnitude below 1 GeV/c.

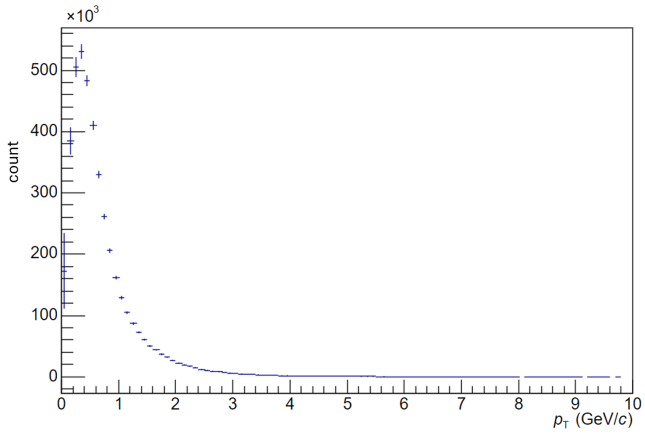

(a) Corrected K^0_S spectra in linear scale.

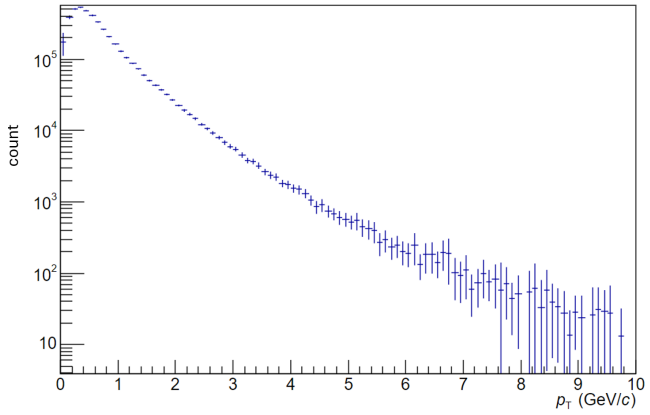

(b) Corrected K^0_S spectra in log scale.

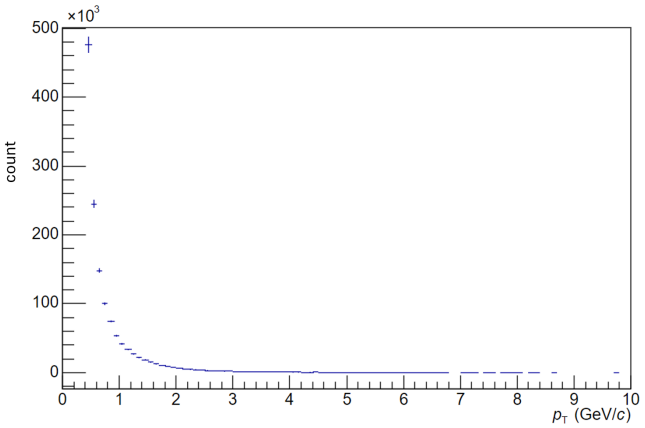

(c) Corrected Λ spectra in linear scale.

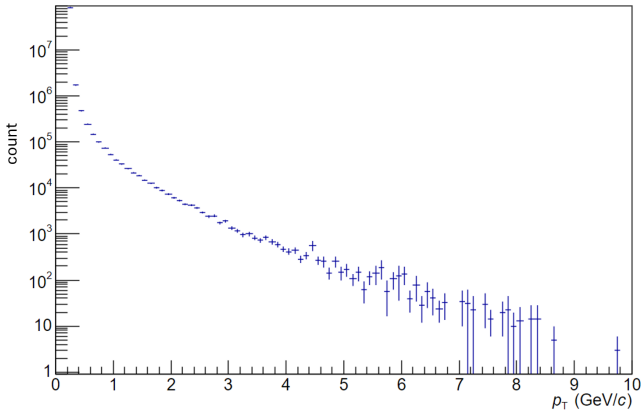

(d) Corrected Λ spectra in log scale.

Figure 7: Corrected V^0 momentum spectra.

Clearly, such an increase in the Λ spectra is unphysical. It indicates the data does not accurately reflect the expected distribution of particles at low transverse momentum. This discrepancy raises concerns about the accuracy of the results and suggests potential issues with either the experimental setup, data collection, or analysis techniques. Despite the observed inconsistencies, further analysis of these results remains valuable. Such analysis could potentially uncover sources of error and expose any contributing factors.

5.2 Baryon to Meson (Λ/K^0_S) Ratio

The p_T dependence of the Λ/K^0_S ratio is frequently investigated in V^0 analysis. The Λ/K^0_S ratio is generally observed to increase as a function of multiplicity at mid p_T [18], which provides insights about the underlying physics of the system. In the absence of multiplicity data, this report will compare the results to previous pp analyses, with the aim of further evaluating the reliability of this investigation. The baryon to meson ratio is shown in figure 8, alongside similar analysis from 2020 [19], which used data collected in June 2015 during ALICE Run 2.

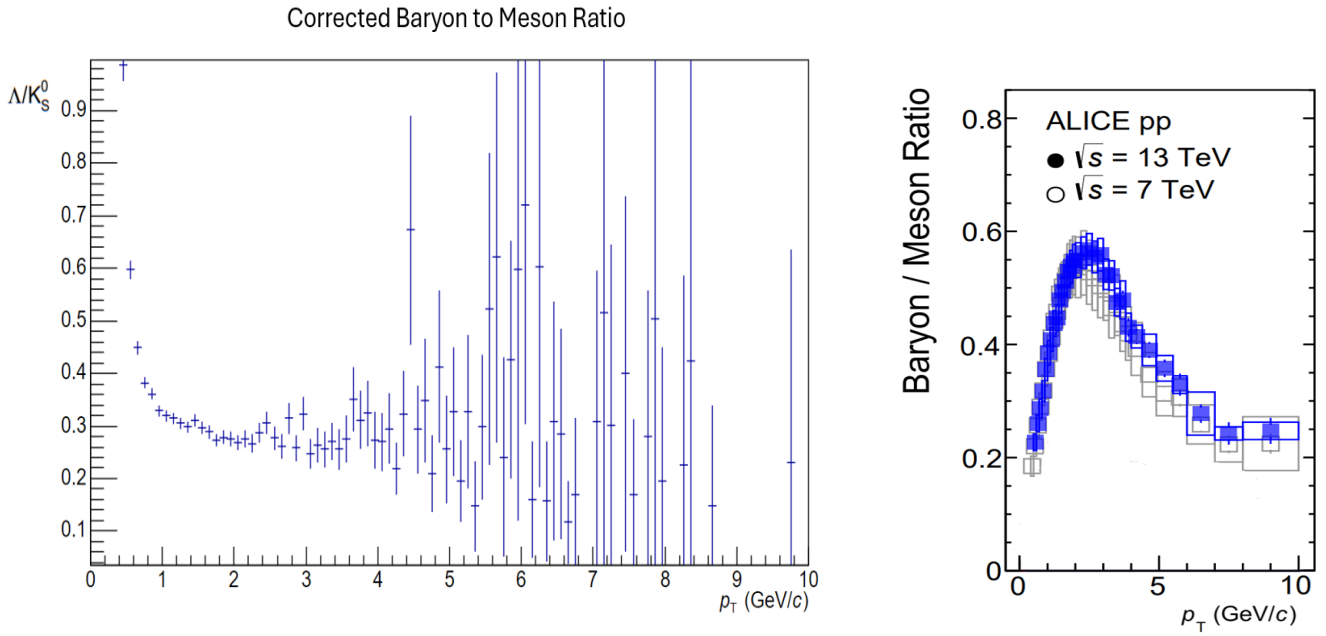

(a) Λ/K^0_S obtained during project.

(b) Λ/K^0_S ratio from Run 2 [19].

Figure 8: Baryon to meson ratio (Λ/K^0_S) as a function of p_T.

At around 1 GeV/c, the ratio is observed to spike, indicating the point at low p_T where the Λ yield starts to increase dramatically relative to K^0_S. After this point, the ratio settles to approximately 0.3. This differs significantly from the ratio obtained from the analysis of Run 2 data, shown in figure 8b, which is seen to increase to a maximum of 0.6 at approximately 2 Gev/c, before tailing off at high p_T. This indicates that the rate of Λ production increases relative to the K^0_S at mid p_T, but that overall, the K^0_S particles are produced in higher quantities across the entire momentum range. Additionally, K^0_S momentum spectra typically extend to lower p_T than Λ spectra, due to the K^0_S mass being closer to the combined mass of its decay products, which leads to the decay occurring

with less available energy and the produced particles having lower momentum. This means that the Λ/K^0_S ratio is expected to tend towards zero at low p_T, as seen in the Run 2 results, and is a key feature missing from the result of the project, shown in figure 8a. A discrepancy of this magnitude between the results and the literature again highlights an issue occurring somewhere in the analysis process.

6 Discussion

The previous section presented the results of the project and discussed the conclusions that may be drawn directly from them. In this section, the particle efficiencies are compared to those obtained from previous results, in an attempt to locate the source of the inconsistencies between the results and the scientific literature. Then a study of the systematic errors introduced during event selection is presented, along with additional comments about possible sources of errors in the project. Finally, additional analysis involving the anti-Lambda ($\bar{\Lambda}$) particle, which may provide insights into possible detector asymmetries, is discussed.

6.1 Efficiency Comparisons

The efficiencies obtained during the project are presented again in figures 9a and 9c, for the K^0_S and Λ respectively, this time keeping their original bin sizes to increase the level of detail shown in the plots. This is compared to the V^0 efficiencies taken from a 2014 PhD thesis [18], which used pp data collected between 2010 and 2011, shown in figures 9b and 9d. The pp collision data relevant for this comparison is located towards the bottom of these plots, as detailed in the legend. Overall, the efficiencies have a similar shape, increasing to a maximum at mid p_T, before decreasing slowly towards the high p_T range. However, previous analysis shows the peaks being located higher and to the right, with the V^0 efficiencies peaking at around 0.3 at 4 GeV/c, compared to around 0.1 at 2 GeV/c for the efficiencies obtained during the project. This shows a factor of three reduction in reconstruction efficiencies for both particles, meaning that if the data is to be believed, the upgraded detector is significantly worse at identifying V^0s.

It must be noted that there were additional cuts on the data used in figures 9b and 9d to just those used in this project, including cuts on the pseudo-rapidity that were slightly tighter than the acceptance of the tracking detectors, and cuts on the lifetime of the V^0s, calculated from the decay radius. The differences in cuts combined with changes to the detector mean that the efficiencies are not expected to be identical between different runs. Regardless, it is still highly unlikely that any differences in cut choices would have affected the reconstruction efficiencies in such a significant manner. More probable however, is a bug or error somewhere in the analysis process, which is causing such significant differences in these results.

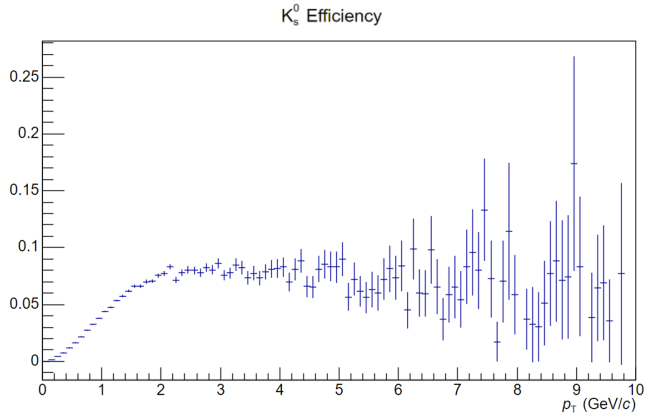

(a) K^0_S efficiency obtained during project.

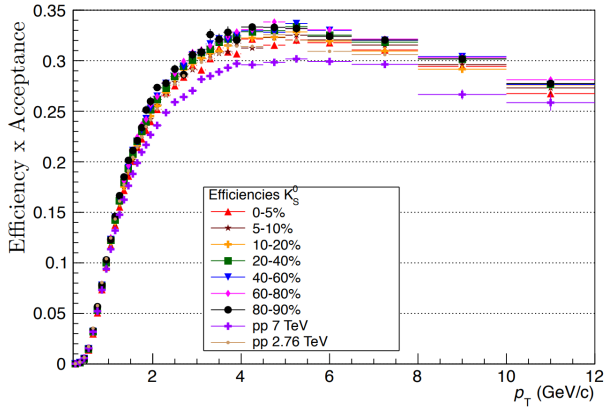

(b) K^0_S efficiency from previous analysis.

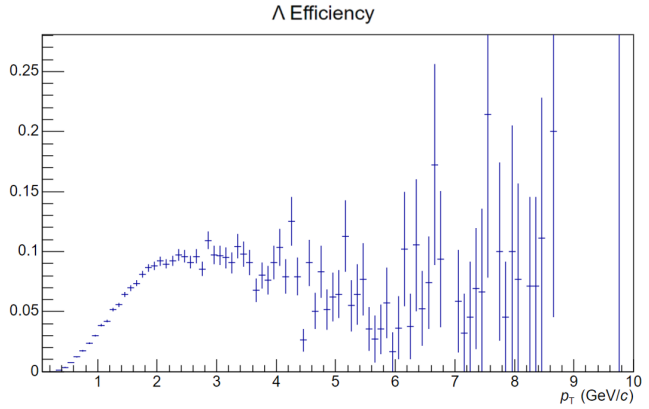

(c) Λ efficiency obtained during project.

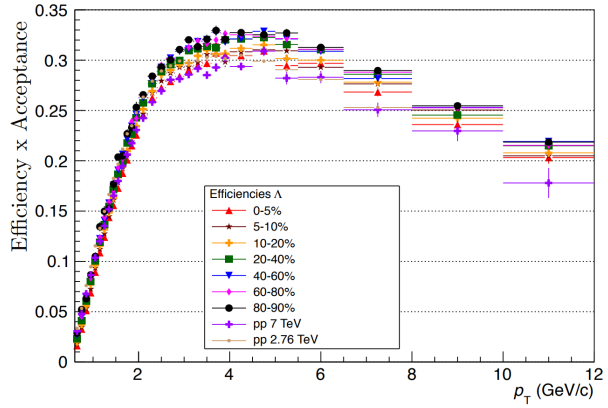

(d) Λ efficiency from previous analysis.

Figure 9: V^0 efficiencies (left) compared to similar efficiency analysis from 2014 (right) [18]. Note, the pp collision efficiencies are towards the bottom of the plots, as detailed in the legend.

6.2 Error Analysis

6.2.1 Systematic cut errors

The event selection process presents an opportunity for systematic errors to be introduced into the data. An idea of these systematic errors may be obtained by comparing the corrected spectra for both particles with the corrected spectra that is obtained while keeping the selection cuts at their loose values. These two plots should be the same, as the loose-cut efficiencies would increase to account for a greater number of particles being accepted. Both V^0 corrected spectra are shown in figure 10, with the blue points corresponding to the loose-cut spectra and the red points corresponding to the optimised-cut spectra. Note a logarithmic scale was used for the Λ plot, to ensure all points were able to be seen. The plot shows that the spectra resulting from the loose cuts is slightly larger relative to the other at low p_T, and this appears to be consistent across both particles.

In order to show the difference between both plots more clearly, the difference between the loose-cut spectra and the optimised-cut spectra is provided below the plots, with the red line showing the point at which both plots are equal. This difference value has then been divided by the optimised-cut value at that point, to effectively normalise it to the histogram's magnitude. This allows it to better show the differences at high p_T, where the absolute differences between the plots are much

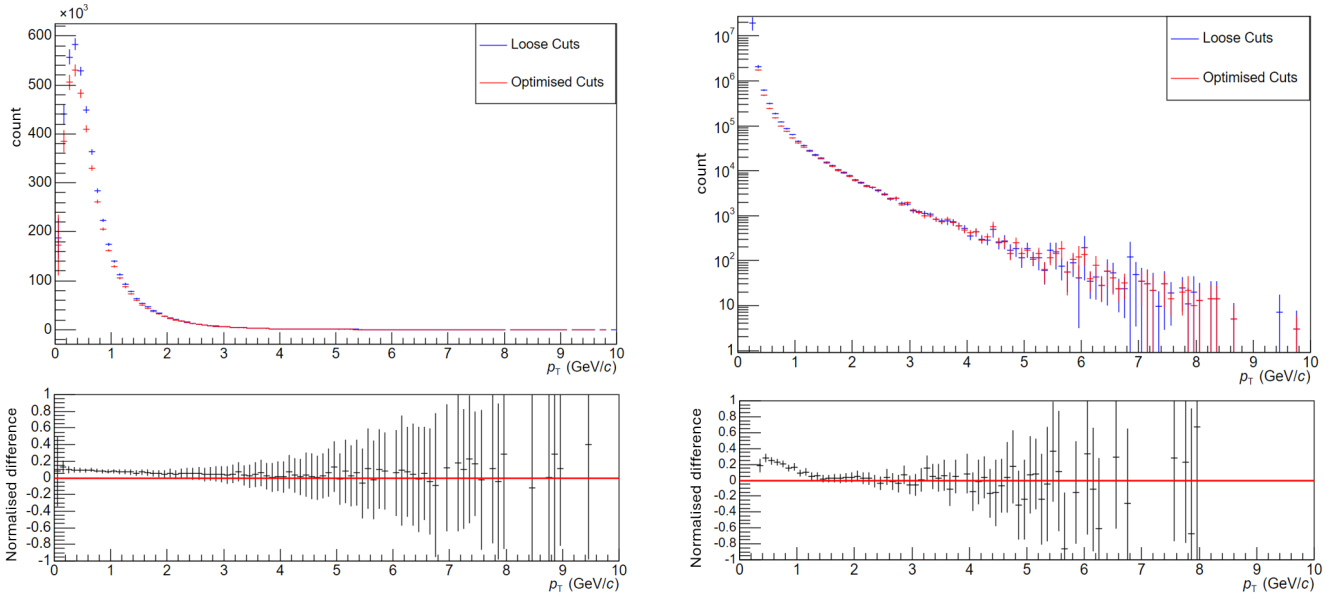

(a) K^0_S corrected spectra on a linear scale

(b) Λ corrected spectra on a log scale

Figure 10: Corrected spectra corresponding to loose (blue) and optimal (red) cuts for both particles. The difference between the two plots is shown beneath, relative to the magnitude of the optimised-spectra.

smaller. At low p_T, this value is around 0.1 for the K^0_S, meaning that the loose-cut spectra is 10% larger than the optimised-cut spectra. This decreases steadily towards zero at around 4 GeV/c, at which point the errors become too large for any meaningful insights to be drawn, as fewer particles are produced in each momentum range resulting in larger statistical uncertainties. Similarly, the loose-cut Λ spectra is larger by up to 30% relative to the optimised-cut spectra at low p_T. Note the log scale makes this difference appear smaller. This decreases to zero at around 1.5 GeV/c, after which point both plots are about the same, within the corresponding error bars.

This shows that the corrected yield is dependent on the exact cut values used, particularly for low p_T, due to the cut variables being imperfectly reproduced by the Monte Carlo simulations. However, this is likely to have a smaller effect on the baryon to meson ratio, as both spectra are correlated. If more time was available, evaluating this dependency for each individual cut would help establish the most unstable cut criteria, and would lead to more informed cut choices being made.

It is also naive to assume that the final cut values used in this project are at the ideal locations, as some of the criteria used to select them, such as the amount of signal retention and MC agreement necessary, were subjective. Furthermore, it is possible that the significance distributions resulting from each cut, would shift slightly depending on the default values used for the remaining cuts. Therefore, once the final set of cuts had been selected, they may then be set as the new default settings, and each cut may be varied slightly to observe any change in the location of the significance peak. This idea was briefly explored, however the change in significance peak was not found to be meaningful. This is something that would be useful to explore further in the future, as the process of updating the default cuts and repeating the cut analysis is iterable, and may be repeated several

times. Overall, it is possible this would lead to a noticeable improvement of results.

6.2.2 Fitting errors

It may be noted that in the mass plots shown previously in figure 3, the fit does not perfectly match the data, falling short of the peak for both particles. In addition, there seem to be non-Gaussian tails of the signal, which exceed the fit on either side of the peak, shown more clearly in the Λ mass plot in figure 3b. This also necessitated the use of a relatively wide 5σ range for signal extraction, to ensure this signal was included. These fitting imperfections meant that there were likely systematic errors on the significance, introduced from imperfect signal and background measurements.

More complex fitting functions were available, which provided a better match to the data and resulted in larger overall significance values from each plot. However, these functions were found to be more volatile and were more likely to fail, especially when fitting the Λ mass plot, which would result in null values in the significance distributions. Since the purpose of the fits was to determine the optimum cut location, only the relative significance from one cut to the next was needed, and the absolute significance for any given cut was not as important. Therefore, the consistency and reliability of the fit was prioritised, leading to a simpler fitting function being used. Overall, the effect of the systematic fitting errors was likely to be small, especially considering the difficulties associated with using more complex functions.

6.2.3 Detector error

The detector itself may introduce sources of error during the data collection process. Firstly, each system has a finite resolution, which tends to worsen for pp collisions as fewer particles are produced. For example, the dE/dx resolution of the TPC is limited to approximately 5% in pp collisions [17]. However, these uncertainties are not enough to explain the issues seen in the results and they impacted previous runs also. However, it is possible that some of the upgraded components are not performing as expected, which may have affected the quality of the data.

6.3 $\bar{\Lambda}/\Lambda$ ratio

The $\bar{\Lambda}$ particle is the anti-matter counterpart to Λ, containing three anti-quarks and decaying into a positive pion and anti-proton ($\bar{p} + \pi^+$). At high enough energies, the production rates of Λ and $\bar{\Lambda}$ become equal due to the interactions the of high-energy quarks and gluons in the system, which lead to processes favouring the production of both particles and their anti-particles. Since there is no initial strangeness in the system, this means that the ratio of the two particles should be unity across the momentum range. Any deviation from unity, would signal the presence of asymmetries in the detector, as it would be more efficient at detecting certain particles compared to their oppositely charged counterparts. Due to technical limitations, $\bar{\Lambda}$ particles were unable to be analysed during this project. A sensible continuation of this project's work would be obtaining a plot of the $\bar{\Lambda}/\Lambda$ ratio, to allow the asymmetries of the detector to be assessed.

7 Conclusion

Overall, the project achieved its initial aim of using preliminary Run 3 data to obtain corrected p_T distributions for both K^0_S and Λ, taking the baryon to meson ratio and comparing these to the scientific literature. This was achieved by successfully implementing selection cuts to enhance the data, and using MC simulations to correct for these cuts and the inefficiencies of the detector itself. However, the results of the project do not match those expected from previous analysis and the cause of this remains unclear. Overall, the V^0 efficiencies obtained were a factor of three lower than expected, and a peculiarity in the Λ corrected spectra at low p_T skewed the baryon-to-meson ratio. These issues could be the result of a bug somewhere in the data collection process, or an error in the subsequent data handling or analysis. Additionally, the upgrades to the detector which preceded ALICE Run 3, may have introduced errors which have yet to be understood.

Logical next steps would be to further assess the effect of the selection cuts on the final results, by analysing each cut criteria individually. This may allow for improved cut choices to be made, leading to more accurate results. In addition, plotting the Λ particle yield relative to its anti-particle, $\bar{\Lambda}$, would reveal possible asymmetries of the detector system, which may have contributed to the observed issues. Ultimately, the project was limited by the absence of multiplicity data, which would have presented further opportunities to study the high-energy physics of collision events, as high multiplicities are often associated with QGP formation.

References

[1] ALICE Collaboration. (1993, 1 March) "Letter of Intent for A Large Ion Collider Experiment at the CERN Large Hadron Collider". CERN/LHCC/93-16/I4. Geneva, Switzerland: CERN.

[2] Reed, R. (for the ALICE Collaboration). (2015). "Jet production in pp, p–Pb and Pb–Pb collisions measured by ALICE". Journal of Physics: Conference Series, 636, 012010.

[3] ALICE Collaboration. (2023). "ALICE upgrades during the LHC Long Shutdown 2". European Organization for Nuclear Research. CERN-EP-2023-009.

[4] Williams, A. G. (2003, 25 May). "Introduction to the Standard Model, QCD and the Lattice". Progress of Theoretical Physics Supplement, No. 151, 21. CSSM, University of Adelaide, SA 5005, Australia.

[5] Marciano, W., & Pagels, H. (1978). Quantum chromodynamics. Physics Reports, 36(3), 137-276. ISSN 0370-1573.

[6] J. Rafelski, & J. Birrell. (2014). "Traveling Through the Universe: Back in Time to the Quark-Gluon Plasma Era". J. Phys.: Conf. Ser. 509 012014

[7] Evans, L., & Bryant, P. (2008, 14 August). "LHC Machine". Journal of Instrumentation, 3(S08001).

[8] Deboy, D., Assmann, R. W., Burkart, F., Cauchi, M., & Wollmann, D. (2011, 29 August). "Acoustic measurements at LHC collimators". LHC Collimation Project.

[9] Y. Hama. (1980). "A Note on Lorentz Transformations and Pseudo-Rapidity Distributions" Jour. Phys. Soc. Jpn. Vol. 50, No. 1, January, 1981, p. 21-23

[10] ALICE Collaboration. (2008). "The ALICE experiment at the CERN LHC". (2008 JINST 3 S08002) Institute of Physics Publishing and SISSA. Published August 14, 2008.

[11] A. Tauro, "ALICE Schematics." General Photo; accessed 17/03/24, May 2017.

[12] ALICE Collaboration, (1999, 18 June). "ALICE Technical Design Report of the Inner Tracking System (ITS)". Geneva, Switzerland: CERN. ISBN 92-9083-144-8.

[13] ALICE Collaboration, "Technical Design Report for the Upgrade of the ALICE Inner Tracking System", Jour. of Phys. G: Nucl. Part. Phys. 41 (2014) 087002.

[14] Reidt, F. (2022). "Upgrade of the ALICE ITS detector". Nuclear Instruments and Methods in Physics Research Section A: Accelerators, Spectrometers, Detectors and Associated Equipment, 1032, 166632

[15] ALICE Collaboration. (2014, 3 March). "Technical Design Report for the Upgrade of the ALICE Time Projection Chamber". ALICE-TDR-016, CERN-LHCC-2013-020.

[16] Veenhof, R. (2003). "Choosing a gas mixture for the ALICE TPC". (Report No. ALICE-INT-2003-29).

[17] W. Yu. (2013, 1 April). "Particle identification of the ALICE TPC via dE/dx". Nuclear Instruments and Methods in Physics Research Section A: Accelerators, Spectrometers, Detectors and Associated Equipment, 706, 55-58.

[18] Hanratty, Luke David. (2014, 13 June) "Λ and K^0_S production in Pb–Pb and pp collisions with ALICE at the LHC." PhD thesis, University of Birmingham.

[19] ALICE Collaboration. (2020, 15 April). "Production of light-flavor hadrons in pp collisions at $\sqrt{s} = 7$ and $\sqrt{s} = 13$ TeV". European Organization for Nuclear Research, CERN-EP-2020-059.